Spectrochimica Acta Part A: Molecular and Biomolecular Spectroscopy 148 (2015) 362–368

Contents lists available at ScienceDirect

Spectrochimica Acta Part A: Molecular and Biomolecular Spectroscopy

journal homepage: www.elsevier.com/locate/saa

Microwave-assisted hydrothermal synthesis and characterization of ZnO nanorods

K. Ocakoglu [a,b], Sh.A. Mansour [c,*], S. Yildirimcan [a], Ahmed A. Al-Ghamdi [d], F. El-Tantawy [e], F. Yakuphanoglu [d,f]

[a] Advanced Technology Research & Application Center, Mersin University, Ciftlikkoy Campus, TR-33343 Yenisehir, Mersin, Turkey
[b] Department of Energy Systems Engineering, Mersin University, Tarsus Faculty of Technology, 33480 Mersin, Turkey
[c] Department of Basic Engineering Science, Faculty of Engineering, Menofia University, Shebin El-Kom, Egypt
[d] Department of Physics, Faculty of Sciences, King Abdulaziz University, Jeddah, Saudi Arabia
[e] Department of Physics, Faculty of Science, Suez Canal University, Ismailia, Egypt
[f] Department of Physics, Faculty of Science, Firat University, Elazig 23169, Turkey

HIGHLIGHTS

- ZnO nanorods of wurtzite phase were synthesized by microwave-assisted hydrothermal route.
- The optical parameters were studied using Kubeleka–Munk approach.
- The obtained optical band gap of the studied sample is 3.17 eV.
- The electrical conductivity mechanism is controlled by thermally activated process.

GRAPHICAL ABSTRACT

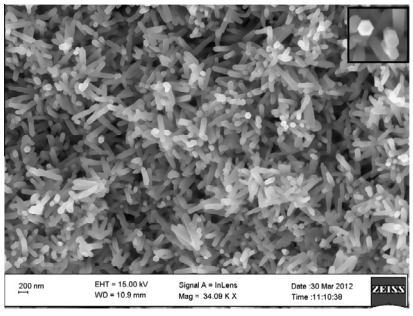

ARTICLE INFO

Article history:
Received 22 September 2014
Received in revised form 25 March 2015
Accepted 27 March 2015
Available online 11 April 2015

Keywords:
ZnO nanorods
Microwave-assisted hydrothermal
Diffuse reflectance
Optical properties

ABSTRACT

For the purpose of this study, the nanorods of zinc oxide were synthesized by rapid microwave-assisted hydrothermal route. The microstructure and surface morphology of the sensitized nanorods were characterized by X-ray diffraction (XRD), field emission scanning electron microscope (FE-SEM) and transmission electron microscope (TEM). XRD results indicate that synthesized ZnO nanorods have wurtzite phase. The calculated value of the particle size using Debye Scherrer formula and Williamson Hall plot was found to be 20–28 nm and 35.3 nm, respectively. Low uniformity distribution of rod-like morphology (60–80 nm in diameter and average length about 250 nm) are seen in TEM micrographs. The optical parameters of the prepared ZnO nanorods have been calculated using Kubeleka–Munk approach for the UV–vis diffuse reflectance spectrum. It is found that the direct transition optical band gap of the studied sample is 3.17 eV. The direct current electrical conductivity (σ) was increased from 6.7×10^{-8} to 3×10^{-7} Ω^{-1} cm^{-1} with increasing the temperature (T) in the range (300–425 K). The obtained variation of σ with T refers that the conductivity mechanism is controlled by thermally activated process.

Introduction

Zinc oxide (ZnO) is a wide band-gap II–VI semiconductor that has attracted resurgent interest as an electronic material for numerous applications. It has attracted much research interest

* Corresponding author.
E-mail address: shehab_mansour@yahoo.com (S.A. Mansour).

http://dx.doi.org/10.1016/j.saa.2015.03.106
1386-1425/

for their unique optical, acoustic, luminescent, electronic and optoelectronic properties. In recent years, many methods have been used to synthesize ZnO material as one-dimensional (1D) nanostructures with different morphologies including nanowires, nanorods, nanoneedles, nanorings, quantum dots and other superstructures [1–8]. The unique properties derived from the unique morphologies would open up new opportunities for ZnO nanomaterials to be used as utilized in various functional devices [9].

ZnO nanomaterials can be synthesized by several well-established synthesis methods, such as sol–gel [10], spray pyrolysis [11], sputtering [12], hydrothermal [13], solvothermal [2] and others. In most cases, the high synthesis temperature leads to the formation of strong aggregates in the ZnO nanomaterials, which subsequently have to be excessively milled resulting in poor control of particle morphology and size distribution [14]. Among of the various synthesis methods of nanomaterials; the hydrothermal technique has several advantages over others synthetic methods, among which are: the one-step synthesis without high temperature calcinations and milling, low aggregation levels and narrow crystallite size distributions, in addition to high purity and excellent control of particle morphology and size [14]. Recently, the hydrothermal microwave-assisted synthesis has attracted wide interests as a novel heating model in material science due to its various advantages including normal atmospheric pressure reacting, short reaction time, rapid heating, low reaction temperature, homogeneous thermal transmission, and the phase purity with better yield [15–18].

In this respect, by considering both the advantage of hydrothermal and microwave-assisted methods, this work focuses on the preparation of ZnO nanorods using microwave-assisted hydrothermal synthesis route. Optical parameters such as; optical energy gap, refractive index and the both parts of complex dielectric constant were studied using Kubeleka–Munk approach for the UV–vis diffuse reflectance spectrum. Moreover, the variation of direct current conductivity with temperature for the synthesized ZnO nanorods were studied.

Experimental procedure

Materials and synthesis

Zinc acetate dehydrate ($Zn(CH_3COO)_2{\cdot}2H_2O$, ⩾98%), sodium hydroxide (NaOH, ⩾98%) and absolute ethanol (CH_3CH_2OH, ⩾99.5%) were purchased from Aldrich. All chemicals were used without further purification.

In a typical one-pot synthesis of ZnO using microwave-assisted hydrothermal method, 5.01 mM of $Zn(CH_3COO)_2{\cdot}2H_2O$ was completely dissolved in 10 mL of distilled water, and then 120 mM NaOH was slowly added into the solution and stirred to form a transparent solution. After adding 100 mL ethanol into the solution, the mixture was loaded into a teflon container. Subsequently, the mixture was radiated (400 W, 100%) at 140 °C for 45 min in a microwave oven (CEM MARS-240/50, frequency 2.45 GHz, maximum power 1600 W), and then cooled at room temperature. The precipitate was filtered and washed with distilled water for several times. Finally, the obtained white solid product was dried in a vacuum furnace at 70 °C for overnight.

Characterizations

The crystal structure of the nanopowders was characterized by a Bruker AXS D8 X-ray diffractometer using Cu K_α radiation (λ = 1.5418 Å) at power of 1600 W (40 kV, 40 mA). The morphology and microstructures of the obtained particles were characterized by transmission electron microscope (TEM), of type JEOL-JEM-1011 operated at 300 kV. Samples for TEM were prepared by air-drying a drop of a dispersed as-product powder in ethanol onto a carbon mesh and then covered with thin film of platinum. Also, field-emission scanning electron microscope (FE-SEM, Zeiss/Supra 55) was used to investigate the morphology of the synthesized samples. Whereas, the elemental analysis of the synthesized nanopowders was checked by energy dispersive X-ray spectroscopy (EDX) unit attached to the FE-SEM. The diffuse reflectance spectrum of the investigated sample was performed using Shimadzu UV–VIS-NIR 3600 spectrophotometer with an integrating sphere attachment. The two-probe method was employed to measure the direct current (dc) conductivity of ZnO nanorods pellet sample. The pellet sample was obtained by applying 5 ton cm^{-2} pressure to form a circular disc with a thickness of about 0.557 mm and a diameter 6.5 mm. The dc conductivity was measured as a function of temperature using Keithley-6517A electrometer. The temperature was controlled using a Lakeshore 331 S temperature controller.

Results and discussion

Structural and morphological characterization of the synthesized ZnO nanostructures

XRD pattern of the prepared ZnO nanopowder sample is shown in Fig. 1. All the diffraction lines are assigned well to wurtzite phase corresponding to the standard crystallographic data in the reference pattern (JCPDS 36-1451), indicating that the synthesized powder was a single phase. In order to calculate the crystalline size (D) of the prepared powder, one can use the value of full width at half maximum (FWHM) for the obtained diffraction peaks using the following known Debye Scherrer equation [19,20]:

$$D = \frac{0.9\lambda}{\beta \cos\theta} \tag{1}$$

where λ, β and θ are the X-ray wavelength, FWHM of the diffraction peak and the Bragg diffraction angle, respectively. The estimated particle size using Debye Scherrer equation for all recorded diffraction lines emerges that the investigated ZnO powder in nano-size between 20 and 28 nm. Whilst, the corresponding value of D for the maximum intensity peak (101) was found to be 28 ± 3 nm.

Although of the Debye Scherrer method is a well known method that uses XRD patterns to predict the crystal size based on FWHM of the diffraction peak, it has not taken in account

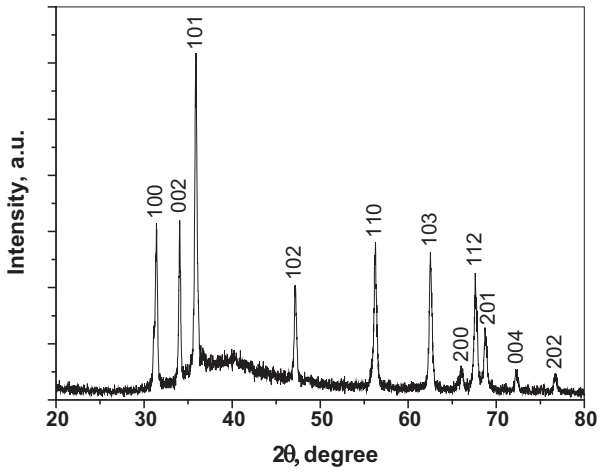

Fig. 1. XRD pattern of the ZnO sample synthesized by microwave-assisted hydrothermal technique.

the peak broadening resulting from the inhomogeneous strain and instrumental effects. In this respect, to known more details about the crystal size of the studied ZnO nanoparticles, one can use Williamson–Hall plot which provide information about lattice strain and effective particle size, particle size with zero strain, present in the sample. Williamson–Hall equation has the form [21]

$$\frac{\beta\cos\theta}{\lambda} = \frac{1}{D_{eff}} + \frac{\mu\sin\theta}{\lambda} \quad (2)$$

where D_{eff} and μ are the effective particle size and the effective strain, respectively. Fig. 2 represents the plot between $\beta\cos\theta/\lambda$ versus $\sin\theta/\lambda$ (Williamson Hall plot). As be seen from Fig. 2, the obtained linear relation has a positive slope which can be attributed to possibility of tensile strain in the investigated ZnO nanoparticles [22]. The calculated value of the tensile strain, slope of the graph, was found to be 0.31%. Whereas, the effective particle size value was calculated to be 35.3 nm.

The TEM micrographs clearly showed the synthesized ZnO in nanorods shape with good uniformity in size and shape as shown in Fig. 3. The nanorods have diameter ranging from 60–80 nm with average length about 250 nm. Fig. 4 shows FE-SEM micrograph of the investigated ZnO nanorods. The obtained FE-SEM micrograph confirmed that, the fabricated ZnO is rod-like crystal. Also, the image of the inset of Fig. 4 emerges that the cross section of the nanorods is hexagonal. Fig. 5 demonstrates the results of the recorded EDX spectrum. The recorded EDX spectrum revealed the high purity of the synthesized ZnO nanorods without detection any impurities.

Optical properties of the fabricated ZnO nanorods

In order to study the optical properties of the synthesized ZnO powder sample, the UV–vis diffuse reflectance spectrum was measured as shown in Fig. 6. This figure reflects the fact that the reflectance spectrum exhibits a strong decrease after wavelength value ~450 nm which can be attributed to optical transitions occurring in the optical band gap.

Determination of the optical band gap

To determine the optical band gap (E_g) of ZnO nanorods sample, the reflectance (R) values can be related to absorption coefficient (α) by applying the Kubeleka–Munk approach throughout the following relation [23]:

$$\alpha = SF(R)/2\upsilon_p \quad (3)$$

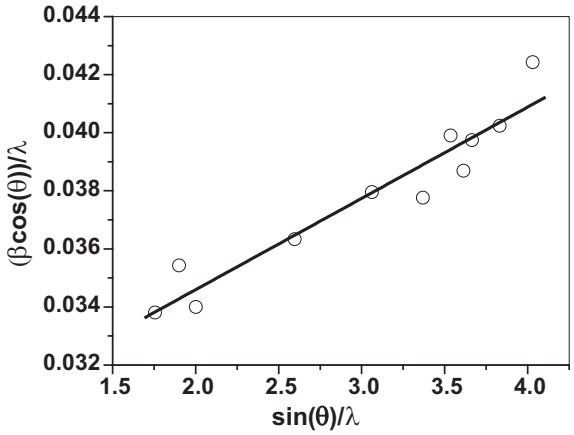

Fig. 2. Williamson Hall plot of the fabricated ZnO sample.

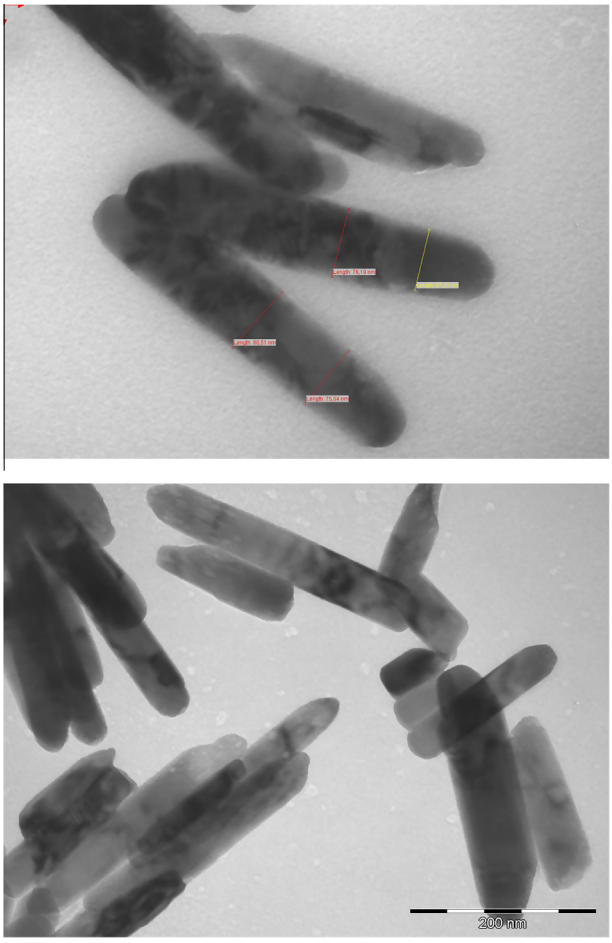

Fig. 3. TEM image of the synthesized ZnO nanorods using microwave-assisted hydrothermal technique.

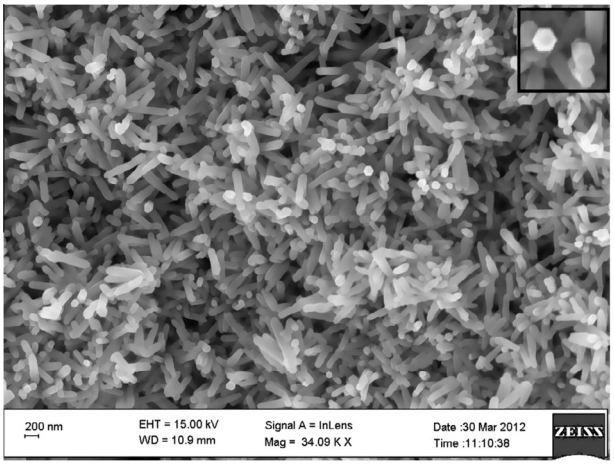

Fig. 4. FE-SEM micrograph of the ZnO nanorods fabricated by microwave-assisted hydrothermal technique. The inset illustrates the hexagonal cross section area of the obtained ZnO nanorods.

where S is the scattering coefficient, υ_p is the volume fraction of the absorbing species and $F(R)$ is the Kubeleka–Munk function which is related to the diffuse reflectance as:

$$F(R) = \frac{(1-R)^2}{2R} \quad (4)$$

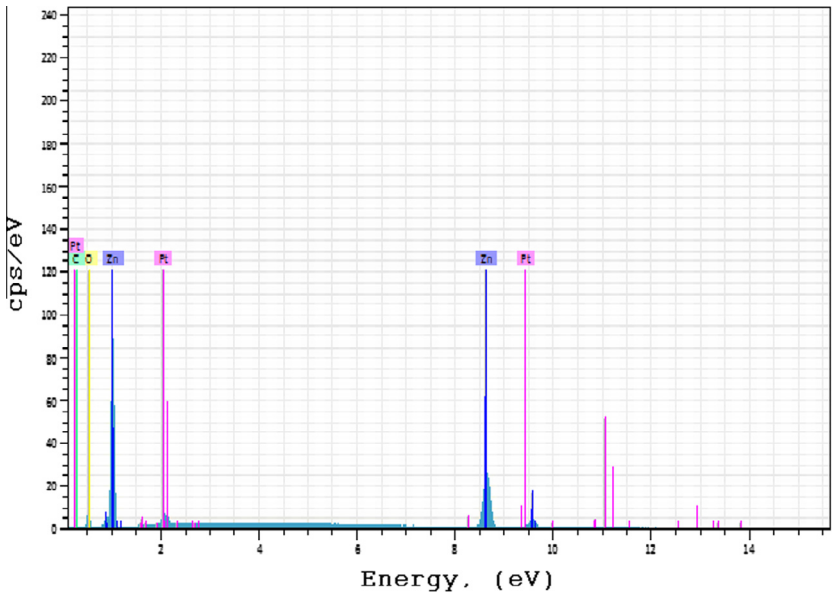

Fig. 5. EDX spectrum of the examined ZnO sample.

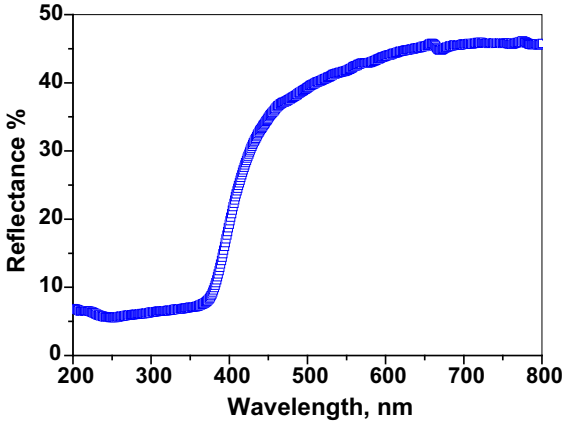

Fig. 6. The reflectance spectrum of the ZnO nanorods fabricated by microwave-assisted hydrothermal technique.

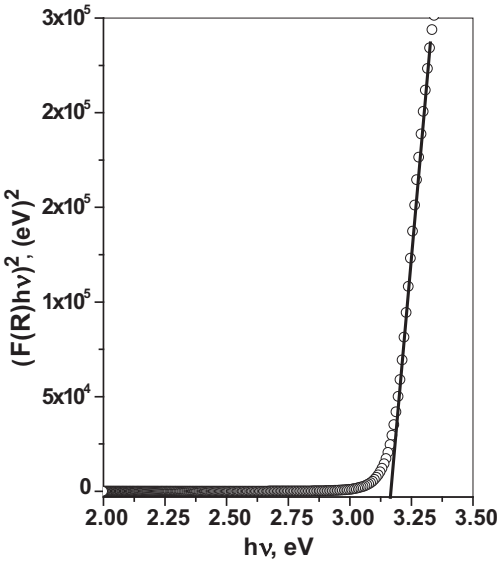

Fig. 7. Plots of $(F(R)h\nu)^2$ versus $h\nu$ for the fabricated ZnO nanorods.

By neglecting the dependence of the scattering coefficient, S, on the scanned wavelength of the incident light, the Kubeleka–Munk function can be reduced to direct proportional relation with absorption coefficient:

$$\alpha = \left(\frac{S}{2\upsilon_p}\right)F(R) = const. \times F(R) \quad (5)$$

So, one can replace the absorption coefficient, α, from the Tauc's equation for direct band gap semiconductors [24], $(\alpha h\nu)^2\alpha(h\nu - E_g)$, by $F(R)$ to be rewritten as:

$$(F(R)h\nu)^2\alpha(h\nu - E_g) \quad (6)$$

A plot of $(F(R)h\nu)^2$ versus $h\nu$ is shown in Fig. 7. The value of optical band gap ($E_g = 3.17$ eV) was determined by extrapolating the linear portion of the plot to $(F(R)h\nu)^2 = 0$. This value of E_g for the investigated ZnO nanorods synthesized by solvothermal is less than that reported for the same technique by Ghoshal et al. [25] (ZnO nanocones with $E_g = 3.315$ eV) and ZnO quantum dots ($E_g = 3.41 : 3.47$ eV) by He and Tsuzuki [2]. Whereas, this obtained value is in a good agreement with that obtained for ZnO nanostructured film prepared by sol–gel deep coating method ($E_g = 3.22$ eV) [10].

By the same token, the estimated band gap of investigated ZnO nanorods sample (3.17 eV) is less than that of bulk ZnO (3.37 eV) [9,26]. Here, is necessary to cite the happening of a blue shift in the spectra of semiconductors in nano size due to the quantum confinement effects. However, the investigated ZnO nanorods sample has E_g value smaller than the bulk one. This effect can be attributed to the chemical defects or vacancies present in the intergranular regions generating new energy level to reduce the band gap energy [27,28].

Refractive index dispersion and dielectric constants Studies

The refractive index, $n(\lambda)$, as function of wavelengths was calculated from diffuse reflectance spectra using the reflectance Fresnel formulae [29]:

$$R = \frac{(n-1)^2 + k^2}{(n+1)^2 + k^2} \tag{7}$$

where n and k is the real part and the imaginary part of the complex refractive index $\tilde{n}$, respectively. Also, the parameter $k = \alpha\lambda/4\pi$ and known as the extinction coefficient. One can solve Eq. (7) using elementary algebraic manipulation to deduce refractive index (n) in the following expression [30]:

$$n = \left(\frac{1+R}{1-R}\right) + \sqrt{\frac{4R}{(1-R)^2} - k^2} \tag{8}$$

The variation of the calculated n values throughout the investigated range of wavelength is shown in Fig. 8. As seen from Fig. 6, the value of n for the fabricated ZnO nanorods varies from 2.3 to 2.66 in the investigated wavelength range. This estimated values of n be close to the reported range of n for ZnO prepared with different techniques. These include: ZnO film prepared by electron beam evaporation (n values from 1.92 to 2.07) [31], ZnO wafer prepared by solvothermal growth technique (n values from 1.92 to 2.23) [32], as well as ZnO nanocrystalline film prepared by DC reactive magnetron sputtering (n values from 1.95 to 2.95) [12]. Fig. 8 also shows that the variation of refractive index values with wavelength has non-monotonic change in wavelength range (300:580 nm), i.e., anomalous dispersion. Then, it varied in a normal dispersion manner for the spectral wavelength range (580:820 nm). This anomalous behavior can be attributed to the resonance effect between the incident electromagnetic radiation and the electrons polarization, which leads to the coupling of electrons in ZnO sample to the oscillating electric field [33].

As being acknowledged, that polarizability of any solid is proportional to its dielectric constant which is related to the density of states within the forbidden gap. So, it is important to see the behavior of the real and imaginary parts of the complex dielectric as a function of the incident photon energy. The complex dielectric constant is defined as; $\tilde{\varepsilon} = \varepsilon_1 + i\varepsilon_2$ and real (ε_1) and imaginary (ε_2) parts of the dielectric constant are related to n and k values throughout the following formulas [30]:

$$\varepsilon_1 = n^2 - k^2, \quad \text{and} \quad \varepsilon_2 = 2nk \tag{9}$$

Fig. 9 shows the variation of ε_1 and ε_2 with the investigated photon energy for the fabricated ZnO nanorods. According to Fig. 9, ε_2 have very small values for whole range of investigated photon energy. This is due to the low value of the extinction coefficient which attributed to highly thickness of the pellet sample (0.557 mm), i.e., highly absorption coefficient. Moreover, Fig. 9 declares that both of the real and imaginary dielectric spectra have

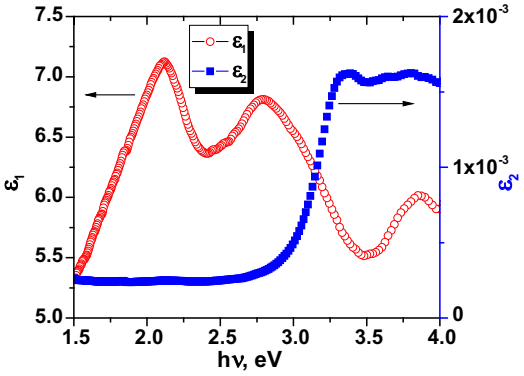

Fig. 9. The variation of real and imaginary part of the dielectric constant with energy for the investigated ZnO nanorods sample.

non-monotonic variation especially ε_1 variation that is more pronounced than ε_2. This trend can be explained by existence of some interactions between photons and electrons within the sample are produced in this energy range [33].

In order to more details about the optical transitions in the studied ZnO nanorods sample, one can apply the Wemple and Didomenico (WD) model [34,35] which depend on a single oscillator description of the frequency-dependent dielectric constant. According to this model, the relation between the refractive index (n), and E_0 which is the single oscillator strength (an average of the optical band gap) below the band gap expressed as:

$$n^2 - 1 = \frac{E_0 E_d}{E_0^2 - E^2} \tag{10}$$

where E_d is the dispersion energy, which is a measure of the intensity of the inter band optical transitions and E is the incident photon energy. So, E_0 and E_d can be determined from plot the relation between $(n^2-1)^{-1}$ versus E^2. Fig. 10 shows the plots of $(n^2-1)^{-1}$ versus E^2. Using the best straight line fitting with $R^2 = 0.98$ both of E_0 and E_d values were calculated and found to be 3.36 eV and 12.75 eV, respectively.

Electrical characterization of the fabricated ZnO nanorods

In order to investigate the electrical conduction mechanism of the synthesized ZnO nanorods, the temperature dependence of the electrical conductivity was studied throughout the temperature range 300–425 K as shown in Fig. 11. This figure declares that the sample has the typical behavior of a semiconductor as its

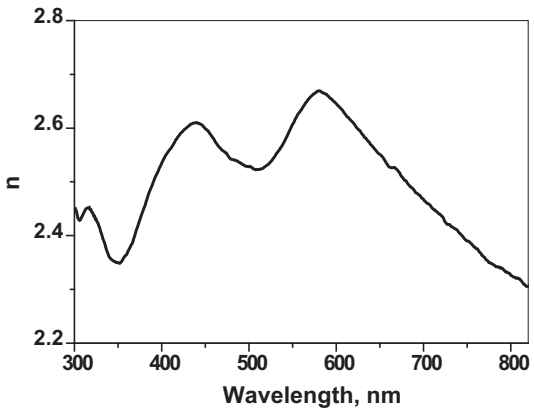

Fig. 8. The dependence of n on the investigated wavelength for the fabricated ZnO nanorods.

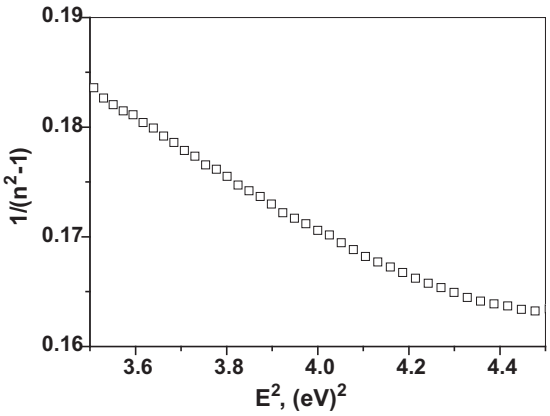

Fig. 10. Plots of $(n^2-1)^{-1}$ versus E^2 for the investigated ZnO nanorods sample.

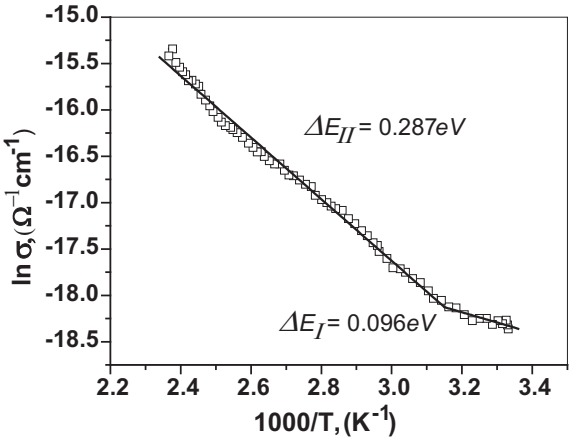

Fig. 11. Temperature dependence of the dc electrical conductivity of the ZnO nanorod pellet. The solid lines represent least-squares fitting.

electrical conductivity increases with increasing temperature. The electrical conductivity at room temperature, σ_{RT}, was found to be $6.7 \times 10^{-8}\ \Omega^{-1}\ cm^{-1}$. This value is in the order with that obtained for ZnO nanoparticles pellet sample prepared by heating of zinc acetate in organic solvent ($3 \times 10^{-8}\ \Omega^{-1}\ cm^{-1}$) [36]. Whilst, this obtained value of σ_{RT} for the studied ZnO nanorods sample is less than that obtained for ZnO single crystal ($\sigma_{RT} = 10^{-3}\ \Omega^{-1}\ cm^{-1}$) reported by Huston [37]. Moreover, the electrical conductivity as shown in Fig. 11 was varied from 6.7×10^{-8} to $3 \times 10^{-7}\ \Omega^{-1}\ cm^{-1}$ in the investigated temperature range (300–425 K) which is less than that recorded for ZnO nanoparticles powder pellet prepared by arrested precipitation method (1.25×10^{-7} to $\sim 10^{-6}\ \Omega^{-1}\ cm^{-1}$ in the temperature range 413–447 K) [38]. Here it is quite appropriate to mention the fact that, the lowest values of the σ for the sensitized nanorods sample may be attributed to grain boundaries interfaces which play important roles in determining the electrical conductivity. In other words, the grain boundaries of nanocrystalline material are in a disordered state which increases the possibility of existence of dislocation defects leading to dangling bonds or other interfacial defects. These defects can act as traps, localized states, between the conduction and valence bands [39].

The function $ln\sigma = f(1/T)$, shown in Fig. 11, indicates two distinct regions of conductivity indicating different mechanisms of conduction and satisfying the thermally activated conductivity formula [40]:

$$\sigma = \sigma_0 \exp\left(\frac{-\Delta E}{kT}\right) \tag{11}$$

where σ_0 is the pre-exponential factor, k is the Boltzmann constant and ΔE is the thermal activation energy for the electrical conductivity. The calculated values of ΔE for the obtained two regions of Fig. 11 were found to be $\Delta E_{II} = 0.287$ eV and $\Delta E_{I} = 0.096$ eV. As being acknowledged, the electrical conduction through ZnO film is mainly by electrons due to oxygen vacancies and Zn interstitial atoms [41]. For the first region (I), the relatively lowest value of activation energy ($\Delta E_I = 0.096$ eV) suggested that the conduction may be due to electrons excited from the shallow donor levels in the band gap of the ZnO semiconductors. Also, the lowest value of the activation energy in the second region ($\Delta E_{II} = 0.287$ eV) than that reported for microphase ZnO (0.5–0.55 eV) and nanophase ZnO of particle size 60 nm is 0.57 eV [42] is attributed to the high density of defects [38].

Conclusions

ZnO nanorods of wurtzite phase have been successfully synthesized by rapid microwave-assisted hydrothermal route for a short reaction time of 30 min. The crystal structure of the obtained product has been verified by XRD and TEM as well as FE-SEM analyses. The calculated particle size value via Debye Scherrer formula as well as Williamson Hall plot confirms that the investigated ZnO sample has nanostructure form. The band gap of the prepared ZnO nanorods has been calculated and was found to be 3.17 eV. This value is smaller than the band gap of the bulk ZnO (3.37 eV) which may be due to the high density of the chemical defects and/or vacancies present in the intergranular regions leading to reduce the band gap energy. The estimated values of the refractive index (2.3–2.66) are comparable with that of other reported work. The dependence of the real and imaginary parts of the dielectric constant on the investigated wavelengths range has been studied and proved to exhibit a non-monotonic behavior. The sensitized ZnO pellet sample shows relatively low electrical conductivity (6.7×10^{-8} to $3 \times 10^{-7}\ \Omega^{-1}\ cm^{-1}$) in the investigated temperature range (300–425 K). These small values of electrical conductivity can be attributed to disordering in the grain boundaries which help increase the density of traps, localized states, due to dislocation or other interfacial defects. The electrical conductivity mechanism of the investigated sample is controlled by thermally activated process with low values of activation energy.

Acknowledgments

The authors, K. Ocakoglu, S. Yildirimcan and F. Yakuphanoglu, thank TUBITAK for the financial support (Grant: 110M803). The authors gratefully acknowledge and thank the Deanship of Scientific Research, King Abdulaziz University (KAU), Jeddah, Saudi Arabia, for the research group "Advances in composites, Synthesis and applications". This work is as a result of international collaboration of the group with Prof. F. Yakuphanoglu.

References

[1] H. Cheng, J. Cheng, Y. Zhang, Q.M. Wang, J. Cryst. Growth 299 (2007) 34.
[2] R. He, T. Tsuzuki, J. Am. Ceram. Soc. 93 (2010) 2281.
[3] S. Sakohara, K. Mori, J. Nanopart. Res. 10 (2008) 297.
[4] N. Kiomarsipour, R.S. Razavi, Superlattices Microstruct. 52 (2012) 704.
[5] S.H. Jung, E. Oh, K.H. Lee, W. Park, S.H. Jeong, Adv. Mater. 19 (2007) 749.
[6] M. Guo, P. Diao, S.M. Cai, Thin Solid Films 515 (2007) 7162.
[7] B.Q. Cao, Y. Li, G.T. Duan, W.P. Cai, Cryst. Growth Des. 6 (2006) 1091.
[8] Y. Ni, G. Wu, X. Zhang, X. Cao, G. Hu, A. Tao, Z. Yang, X. Wei, Mater. Res. Bull. 43 (2008) 2919–2928.
[9] U. Ozgur, Ya.I. Alivov, C. Liu, A. Teke, M.A. Reshchikov, S. Dogan, V. Avrutin, S.G. Cho, H.A. Morkoc, J. Appl. Phys. 98 (2005) 041301.
[10] Sh.A. Mansour, F. Yakuphanoglu, Solid State Sci. 14 (2012) 121.
[11] M.J. Height, L. Madler, S.E. Pratsinis, F. Krumeich, Chem. Mater. 18 (2006) 572.
[12] W.X. Cheng, A.L. Ding, X.S. Zheng, P.S. Qiu, X.Y. He, J. Phys.: Conf. Ser. 152 (2009) 012036.
[13] S. Baruah, J. Dutta, Sci. Technol. Adv. Mater. 10 (2009) 013001.
[14] W.L. Suchanek, J. Cryst. Growth 312 (2009) 100.
[15] Z. Zhu, D. Yang, H. Liu, Adv. Powder Technol. 22 (2011) 493.
[16] C.C. Wu, C.Y. Shiau, D.W. Ayele, W.N. Su, M.Y. Cheng, C.Y. Chiu, B.J. Hwang, Chem. Mater. 22 (2010) 4185.
[17] P.G. Sheikhi Abadi, M. Salavati-Niasari, F. Davar, Superlattices Microstruct. 53 (2013) 76.
[18] F. Al-Hazmi, N. Abdel Aal, A.A. Al-Ghamdi, F. Alnowaiser, Z.H. Gafer, A.G. Al-Sehemi, F. El-Tantawy, F. Yakuphanoglu, J. Electroceram. 31 (2013) 324.
[19] P. Scherrer, Nachr. Ges. Wiss. Göttingen 26 (1918) 98.
[20] J.I. Langford, A.J.C. Wilson, J. Appl. Cryst. 11 (1978) 102.
[21] G.K. Williamson, W.H. Hall, Acta Metall. 1 (1953) 22.
[22] V. Senthilkumar, P. Vickraman, M. Jayachandran, C. Sanjeeviraja, J. Mater. Sci.: Mater. Electron. 21 (2010) 343.
[23] G. Kortum, Reflectance Spectroscopy, Springer-Verlag, New York, 1969.
[24] J. Tauc, R. Grigorov, A. Vancu, Phys. Status Solidi 15 (1966) 627.
[25] T. Ghoshal, S. Kar, J. Ghatak, S. Chauduri, Mater. Res. Bull. 43 (2008) 2228.
[26] A.B. Djurisic, Y.H. Leung, Small 2 (2006) 944.
[27] H. Yamamoto, S. Tanaka, K. Hirao, J. Appl. Phys. 93 (2003) 4159.

[28] L. Soriano, M. Abbate, A. Fernandez, A.R. Gonzalez-Elipe, J.M. Sanz, Chem. Phys. Lett. 208 (2003) 460.
[29] N.A. Subrahamanyam, A Textbook of Optics, Brj Laboratory, Delhi, 1977.
[30] T.S. Moss, G.J. Burrell, E. Ellis, Semiconductor Opto-Electronics, Butterworths, London, 1973.
[31] N.R. Aghamalyan, I.A. Gambaryan, E.Kh. Goulanian, R.K. Hovsepyan, S.I. Kostanyan, R.B. Petrosyan, E.S. Vardanyan, A.F. Zerrouk, Sci. Technol. 18 (2003) 525.
[32] D. Ehrentraut, H. Sato, Y. Kagamitani, H. Sato, A. Yoshikawa, T. Fukuda, Prog. Cryst. Growth Charact. Mater. 52 (2006) 280.
[33] D.T. Phan, A.A.M. Farag, F. Yakuphanoglu, G.S. Chung, J. Electroceram. 29 (2012) 12.
[34] M. Didomenico, S.H. Wemple, J. Appl. Phys. 40 (1969) 720.
[35] M. Didomenico, S.H. Wemple, Phys. Rev. B. 3 (1971) 1338.
[36] N. Naeem, S.K. Hasanah, A. Mumtaz, J. Phys.: Condens. Matter 20 (2008) 025210.
[37] A.R. Huston, Phys. Rev. Lett. 4 (1960) 505.
[38] J. Jose, M. Abdul Khadar, Mater. Sci. Eng. A Struct. 304–306 (2001) 810.
[39] J. Jose, M. Abdul Khadar, Nanostruct. Mater. 11 (1999) 1091.
[40] N.F. Mott, E.A. Davis, Electronic Processes in Non-Crystalline Materials, 2nd ed., Oxford University Press, UK, 1979.
[41] C. Kilic, A. Zunger, Phys. Rev. Lett. 88 (2002) 095501.
[42] J. Lee, H. Hwang, J.J. Mashek, T.O. Mason, A.E. Miller, R.W. Siegel, J. Mater. Res. 10 (1995) 2295.